

# Journal of Materials Chemistry A

Accepted Manuscript



This is an *Accepted Manuscript*, which has been through the Royal Society of Chemistry peer review process and has been accepted for publication.

*Accepted Manuscripts* are published online shortly after acceptance, before technical editing, formatting and proof reading. Using this free service, authors can make their results available to the community, in citable form, before we publish the edited article. We will replace this *Accepted Manuscript* with the edited and formatted *Advance Article* as soon as it is available.

You can find more information about *Accepted Manuscripts* in the [Information for Authors](#).

Please note that technical editing may introduce minor changes to the text and/or graphics, which may alter content. The journal's standard [Terms & Conditions](#) and the [Ethical guidelines](#) still apply. In no event shall the Royal Society of Chemistry be held responsible for any errors or omissions in this *Accepted Manuscript* or any consequences arising from the use of any information it contains.

Cite this: DOI: 10.1039/c0xx00000x

www.rsc.org/xxxxxx

ARTICLE TYPE

## ***In-situ* Growth of FeS Microsheet Networks with Enhanced Electrochemical Performance for Lithium-Ion Batteries**

Chengcheng Xing,<sup>\*a</sup> Dan Zhang,<sup>\*a</sup> Ke Cao,<sup>a</sup> Shumin Zhao,<sup>b</sup> Xin Wang,<sup>b</sup> Haiying Qin,<sup>b</sup> Jiabin Liu,<sup>\*a</sup>  
Yinzhu Jiang<sup>\*a</sup> and Liang Meng<sup>a</sup>

Received (in XXX, XXX) Xth XXXXXXXXXX 20XX, Accepted Xth XXXXXXXXXX 20XX

DOI: 10.1039/b000000x

A facile solution-based approach has been developed for the preparation of mackinawite FeS microsheet networks directly on Fe foil. It is found that sulfur sources significantly impact the uniformity and purity of the products, while ethylenediamine as a strong donor ligand plays an important role in the formation of FeS microsheet networks. As comparison, numerous FeS microspheres are obtained in the absence of ethylenediamine. The FeS microsheet networks deliver promising Li storage capacity (772 mAh g<sup>-1</sup> at the 1<sup>st</sup> cycle and 697 mAh g<sup>-1</sup> at the 20<sup>th</sup> cycle), much higher than that of the FeS microspheres. The enhanced electrochemical performance of the FeS microsheet networks can be attributed to their layered structure and unique morphology, which possesses larger electrode-electrolyte contact area, shorter diffusion length of the ions and easier transportation of the electrons.

\* Corresponding author. Tel.: +86 57187951027; fax: +86 57187952358.

E-mail address: [liujiabin@zju.edu.cn](mailto:liujiabin@zju.edu.cn), [yziang@zju.edu.cn](mailto:yziang@zju.edu.cn)

Cite this: DOI: 10.1039/c0xx00000x

www.rsc.org/xxxxxx

## ARTICLE TYPE

## 1 Introduction

Layered transition-metal sulfides are theoretically and technologically important materials due to their interesting electronic,<sup>1</sup> electro-chemical<sup>2-5</sup> and optical<sup>6,7</sup> properties resulting from their low dimensionality. Two-dimensional (2D) nano/micro sheets of these layered-structured metal sulfides can be obtained through direct growth or exfoliation due to their weak interlayer bonds. There have been some pioneer works for the direct growth of ultrathin mackinawite-type FeS nanosheets,<sup>8</sup> greigite-type Fe<sub>3</sub>S<sub>4</sub> nanoplatelets<sup>9</sup> and ultrathin MoS<sub>2</sub> sheets<sup>10</sup>. However, they are usually harvested in powder form, which is susceptible to dissolve, agglomerate, and sinter when they are used for the fabrication of thin-films. It is necessary to explore a facile approach to grow 2D nanostructured metal sulfides directly on a substrate.

2D nanostructure of some layered-structured metal sulfides such as MoS<sub>2</sub><sup>11,12</sup> and WS<sub>2</sub><sup>13</sup> have been previously studied in energy storage systems due to their unique structural and surface properties. However, the metal elements in these sulfides are relatively heavy, which may limit their theoretical specific energy densities.<sup>14</sup> Among metal sulfides, iron sulfides have attracted great attention due to their cost effectiveness and abundance in nature. They have been explored as a material for microbial fuel cells<sup>15</sup> and as a substrate for the removal of toxic trace metals from water<sup>16</sup>. Also, iron sulfides are suitable electrodes for thermal primary batteries<sup>17</sup> and lithium ion batteries (LIBs)<sup>18-20</sup> because of their high theoretical capacities of 609 mA h g<sup>-1</sup> for FeS and 894 mA h g<sup>-1</sup> for FeS<sub>2</sub>.<sup>21,22</sup> However, the main drawback of these electrode materials stems from the huge volume expansion-contraction caused by the lithiation and delithiation processes. For example, the reduction of FeS to Fe and Li<sub>2</sub>S leads to a 200% volume expansion, leading to pulverization and thus a loss of electrical contact.<sup>23</sup> 2D nanostructured electrodes have been confirmed to well sustain the volume change and thus benefit for the integrity of electrode during cycling. Zheng's group have reported that the 2D structure and large amounts of mesopores within the nanosheets can effectively improve structural stability, reduce the diffusion length for lithium ions and electrons, and buffer volume expansion during cycling.<sup>24</sup> Xu *et al.*<sup>14</sup> also confirmed the nanosheets can effectively accommodate large volume changes induced during the charge/discharge process. Furthermore, an intimate electric contact between the electrode and current collector, which can be realized by the direct growth of electrode materials on current collectors, is also extremely important both for fast electrochemical reactions and prolonged cycling behaviour.<sup>25</sup>

Herein, we report a facile solution-based approach for the *in-situ* growth of FeS microsheet networks on iron foil, which exhibits improved lithium storage performance. It was found that the sulfur sources have significant impact on controlling the

uniformity and purity of the final products, while ethylenediamine (EDA) as a strong donor ligand plays an important role in the formation of FeS microsheet networks. The formation mechanism of the 2D FeS nanostructured films is proposed according to time-dependent experiments and adjusted synthesis conditions. Benefitted by the 2D layered structures of mackinawite FeS and direct growth of vertically-aligned structures on iron foil, the FeS microsheet networks exhibited notably improved capacity performance for LIBs.

## 2 Results and discussion

### 2.1 Microstructure

Fig. 1a shows the XRD patterns of the FeS microsheet networks. All the diffraction peaks can be well indexed as the mackinawite FeS (PDF No. 86-0389), except for three additional peaks corresponding to the iron foil substrate. The strong and sharp diffraction peaks imply that the FeS microsheet networks are highly crystallized. It should be noted that the strongest peak in the FeS microsheet networks is not (001) suggested by the standard PDF card, but (110) and (200), indicating the favored growth orientation of the FeS microsheet networks. In comparison, the FeS microspheres exhibit similar XRD patterns (Fig. 1b) as the FeS microsheet networks, which also match well with the patterns of mackinawite. However, the intensities of most peaks are in consistent with the standard powder mackinawite patterns, indicating that there is no texture or favored orientation for FeS microspheres.

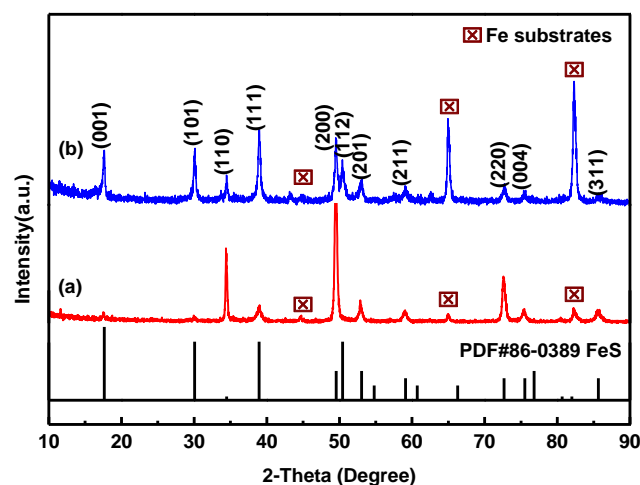
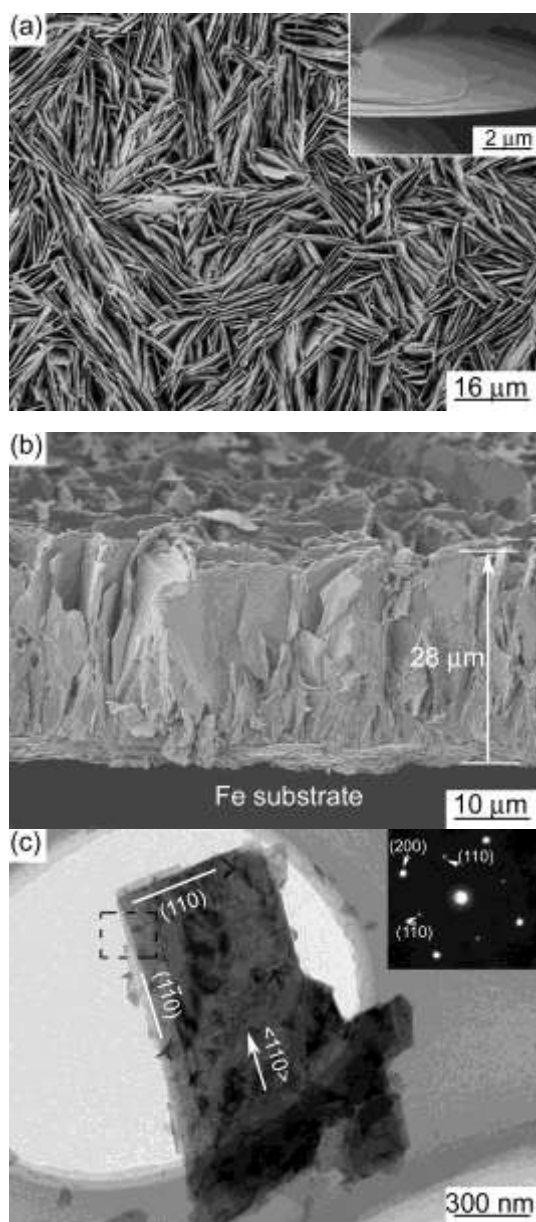


Fig.1 XRD patterns of the FeS products (a) microsheet networks and (b) microspheres.

The FeS microsheet networks were further characterized by FESEM and TEM as illustrated in Fig.2. FeS microsheets are formed in network-like structure on a large scale area (Fig. 2a).

Additionally, a single microsheet is assembled by several nanosheets as depicted in the insert image in Fig. 2a. Typical cross-section FESEM image (Fig. 2b) clearly shows those microsheets nucleate from the Fe substrate and grow up vertically with a height of 20~25  $\mu\text{m}$ . An individual FeS nanosheet with two perpendicular surfaces is clearly shown in TEM image (Fig. 2c). Meantime, the corresponding selected area electron diffraction (SAED) patterns are given as an insert in Fig. 2c, the two perpendicular surfaces could be indexed as (110) and  $(\bar{1}\bar{1}0)$  respectively. The HRTEM image of the region highlighted by a black rectangle in Fig. 2c is shown in Fig. 2d. The lattice planes are clearly observed and indexed as (110),  $(\bar{1}\bar{1}0)$  and (200). The TEM observation suggests that the FeS microsheets are surrounded by the {110} planes, which is in well agreement with the XRD results that (110) peak of FeS microsheet has an abnormal strong intensity (Fig. 1a). Based on the TEM characterization, the morphology and the growth orientation of the FeS microsheet can be illustrated in Fig. 1e.



**Fig.2** FESEM images of FeS microsheet networks viewed from (a) the top-view and (b) cross-section, (c) TEM image of a single FeS nanosheet, inset is the corresponding SAED patterns and (d) HRTEM image of the region highlighted by a black rectangle in Fig. 2c, (e) schematic drawing showing the typical morphology of the FeS microsheet.

Replacing  $\text{Na}_2\text{S}$  and S powder with Tu as the sulfur source in the absence of EDA and keeping other synthesis parameters similar will lead to the growth of FeS microspheres. A panoramic FESEM image in Fig. 3a displays that the diameter of the FeS microsphere is 2-5  $\mu\text{m}$ . The high-magnification FESEM image (Fig. 3b) illustrates that the surface of the FeS microsphere is not smooth and it is built by numerous microsheets. Typical image of an individual FeS microsphere was shown in Fig. 3c. The corresponding SAED patterns consist of several rings, suggesting the polycrystalline characteristics. Fig. 3d shows the HRTEM image of the edge of the microsphere. Several nanograins with different orientation are clearly observed, which also confirms the polycrystalline characteristics of the FeS microsphere.

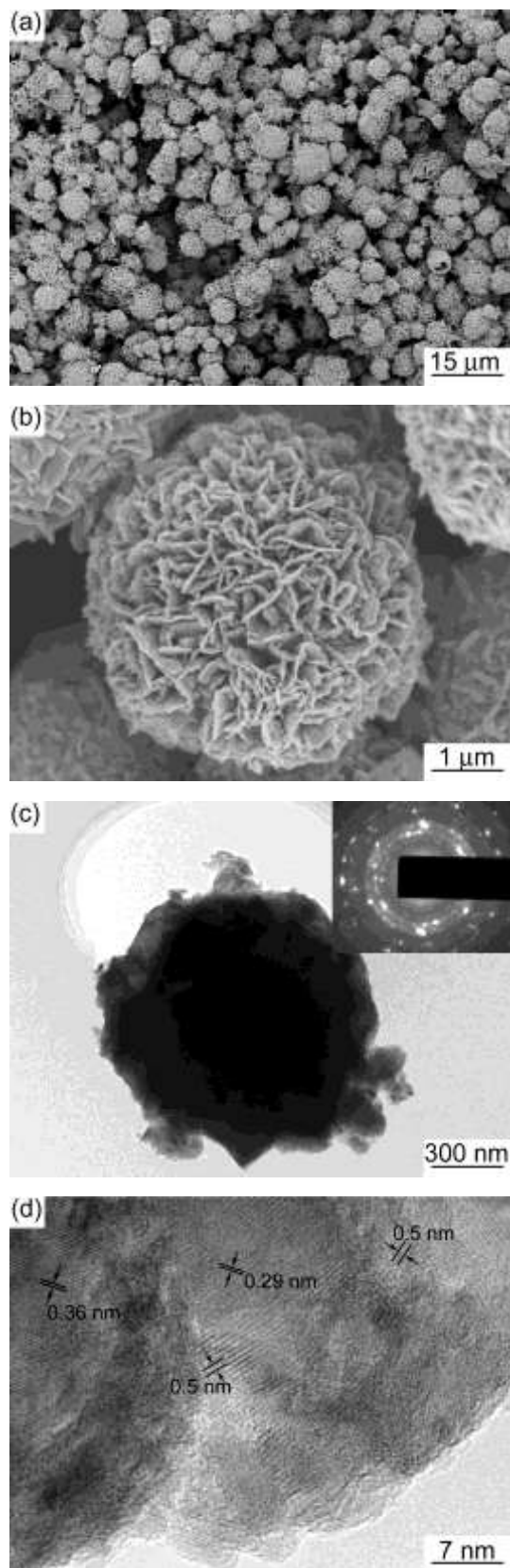


**Fig.3** (a) and (b) FESEM images of FeS microspheres; (c) TEM image of a single microsphere, insert is the corresponding SAED patterns and (d) HRTEM image of the edge of the microsphere.

## 2.2 Possible growth mechanism of the FeS films

In order to clarify the formation mechanism of the FeS microspheres on Fe foil, the products grown for various periods were investigated by FESEM. After reaction for 4 h, a gray film was obtained and many nanosheets appeared clearly on the Fe surface (Fig. 4a). When the reaction time was extended to 6 h, the size and number of nanosheets increased and spread uniformly on the substrate (Fig. 4b). When the reaction time was further increased to 9 h, the microspheres grew larger and fully covered the substrate and became dense to form a net-like film (Fig. 4c), which similar to that obtained at 12 h. The FeS film did not detach from the Fe foil, even after long periods of intense ultrasonication, suggesting that the film strongly adhered to the substrate. This strong adhesion was presumably due to the *in-situ* growth of FeS nanosheet from the Fe foil.

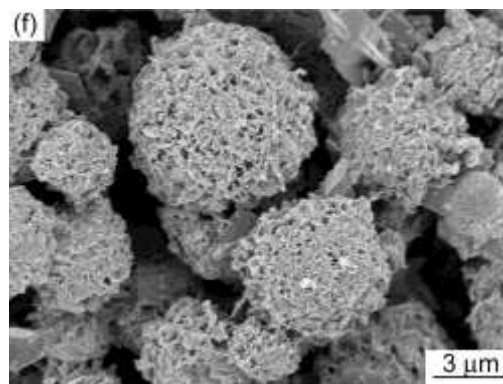
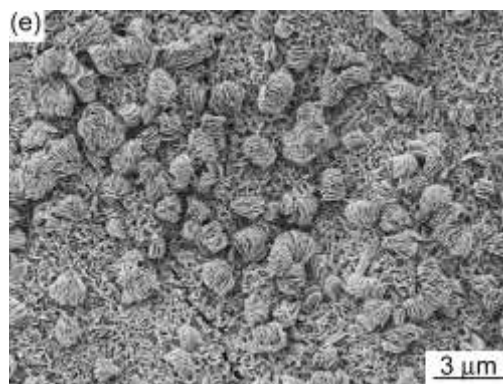
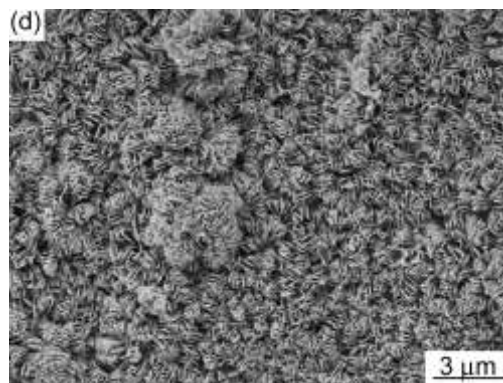
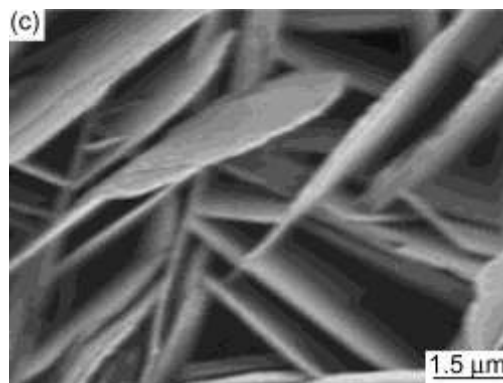
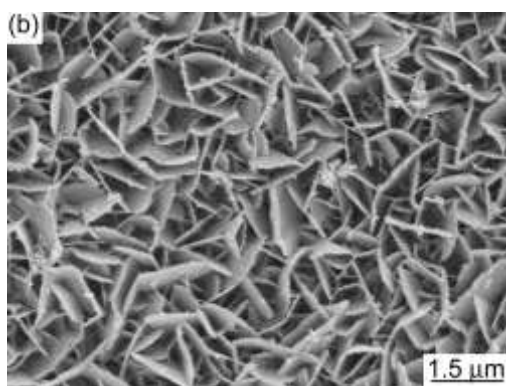
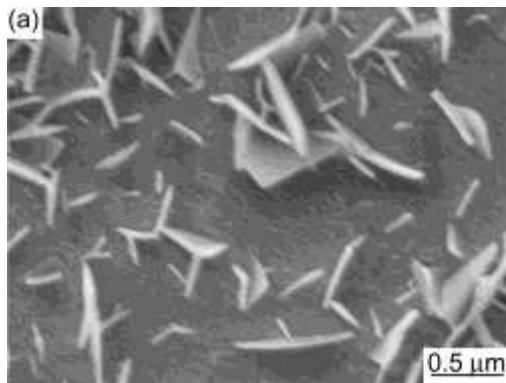
Similar time-dependent experiments were carried out to investigate the formation and evolution of the FeS microspheres. As shown in Fig. 4d, at the early reaction stage, the products were composed of numerous nanosheets which were uniformly and densely distributed on the substrate. When the reaction time was extended to 6 h, the nanosheets grew larger and tend to aggregate together to form flower-like products (Fig. 4e). When the reaction was further prolonged to 9 h, the microsphere-like product fully formed, as displayed in Fig. 4f. The FESEM observation indicates that the nanosheets gradually aggregated into microspheres with increasing reaction time. These processes seem to obey the Ostwald ripening mechanism, as they were driven by decreasing the surface energy to form a densely packed morphology.

The growth of FeS nanosheet networks and FeS microspheres is schematically illustrated in Fig. 4g. The uniform nanosheet networks were successfully obtained with  $\text{Na}_2\text{S}\cdot 9\text{H}_2\text{O}$  and S powder as sulfur sources in the presence of EDA (Fig. 2a). A likely reaction pathway is that  $\text{Fe}^{3+}$  in precursor solution reacts with Fe foil to form  $\text{Fe}^{2+}$ :  $2\text{Fe}^{3+} + \text{Fe} \rightarrow 3\text{Fe}^{2+}$  (4).<sup>26</sup> Then  $\text{Fe}^{2+}$  likely reacts with EDA to form  $[\text{Fe}(\text{EDA})_m]^{2+}$  ( $m > 0$ ). At the same time, some S in solution reacts with  $\text{Na}_2\text{S}$  to form  $\text{S}_2^{2-}$ , and other S steadily supplies  $\text{S}^{2-}$  in a controllable way. Then,  $\text{S}_2^{2-}$  and  $\text{S}^{2-}$  react with  $[\text{Fe}(\text{EDA})_m]^{2+}$  to form FeS-*m*EDA nuclei layers for uniform FeS nanosheet in the EDA-sufficient precursor.<sup>9</sup> The shape of the crystalline FeS sheets may be directly related to the crystal lattice structure of the mackinawite phase instead of the influence of solvents. Mackinawite adopts a layered structure that are held together through Van Der Waals interactions, leading to the growth within the (001) plane.<sup>8, 27</sup> This is consistent with nanosheets of mackinawite-type FeS that are truncated along the [001] direction, and further indicates that the nanosheet morphology is characteristic of the bulk of the sample.

To investigate the effect of the EDA and sulfur sources on the obtained products, we carried out the synthesis of FeS under different conditions. When we substituted Tu for  $\text{Na}_2\text{S}\cdot 9\text{H}_2\text{O}$  and S in the presence of EDA, flower-like microspheres products with poor orientation was obtained as shown in Figure S2a. The likely reaction pathway is that thiourea reacts with  $\text{H}_2\text{O}$  in the system to produce  $\text{S}^{2-}$ , which bonds with  $[\text{Fe}(\text{EDA})_m]^{2+}$  in solution to form FeS-*m*EDA. XRD (Figure S2b) studies suggest that the layered structured products contain not only mackinawite FeS, but also

some impurities ( $\text{Fe}_{1-x}\text{S}$ ). Wang *et al.*<sup>28</sup> indicated that the poor orientation of the microsheet and the existence of impurities would be due to the reaction being too fast to control at high temperature when Tu was used as the sulfur source.

5 It is well-known that solvent plays an important role in determining the final morphology of crystals. Various solvents with different chemical and physical properties can affect the reactivity, solubility and diffusion behavior of the reactants. The coordinating ability and polarity of the solvents have a great  
10 influence on the crystal morphology of the final product in particular.<sup>29,30</sup> The EDA molecules have the strong coordinating ability and function as metal activation (chelation) or mediating the electron transfer in the reaction system. These molecules enable the forming of chemically stable coordinating metal  
15 complexes with metal ions and such metal complexes will perform as the intermediate species in the chemical reaction.<sup>31,32</sup> Furthermore, Lu *et al.*<sup>33</sup> found that EDA was a strong donor ligand due to its N-chelating behavior and it played an important role in the formation of 2D ZnS nanobelt arrays. As a result, the  
20 FeS-EDA molecular precursors may serve as molecular templates in the control of the crystal growth, which is lead to the microsheet networks obtained in the presence of EDA.<sup>31,34,35</sup> Replacing EDA with  $\text{H}_2\text{O}$  as solvents leads to the change of growth significantly and finally the nanosheet aggregates into  
25 spheres to minimize the surface energy. It is found that the sulfur sources and the EDA have a significant effect on the growth mechanism of the FeS nanostructured films, which is schematically illustrated in Fig. 4 (g).



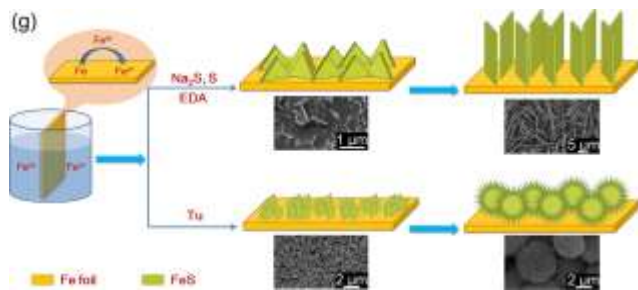


**Fig.4** FESEM images of the FeS microsheets obtained at 160 °C at different stages: (a) 4 h, (b) 6 h, (c) 9 h; FeS microspheres obtained at 160 °C at different stages: (d) 3 h, (e) 6 h, (f) 9 h; (g) schematic mechanism for the fabrication process of FeS microsHEET networks and FeS microspheres on Fe foil.

### 2.3 Electrochemical performance

The electrochemical properties of FeS microsHEET networks and microspheres as anode electrodes in lithium-ion storage were tested based on two-electrode coin-type cells with Li metal as the counter-electrode. Fig. 5a shows the cyclic voltagrams (CVs) of the FeS microsHEET networks electrode at a scan rate of 0.1 mV s<sup>-1</sup> between 0.01 and 3 V. At the 1<sup>st</sup> cycle, three reduction peaks appear obviously at 1.2, 1.15 and 0.5 V, while only one oxidation peak is shown at 2.0 V. The small peak at 1.2 V is related to the formation of Li<sub>2</sub>FeS<sub>2</sub><sup>21, 36</sup>: 2FeS + 2Li + 2e<sup>-</sup> = Li<sub>2</sub>FeS<sub>2</sub> + Fe (1) and the sharp peak at around 1.15 V accounts for the conversion reaction<sup>37</sup>: FeS + 2Li + 2e<sup>-</sup> = Li<sub>2</sub>S + Fe (2). The broad peak at 0.5 V is attributed to the decomposition of the electrolyte and formation of a solid electrolyte interlayer (SEI). Fong *et al.*<sup>38</sup> indicated that the peak at around 2.0 V might correspond to the oxidation of Fe to form Li<sub>2-x</sub>FeS<sub>2</sub> as Fe + Li<sub>2</sub>S - xLi - xe<sup>-</sup> → Li<sub>2-x</sub>FeS<sub>2</sub> (3). The cathodic peak shifts to 1.3 V for the 2<sup>nd</sup> cycles, which mainly originates from the irreversible insertion reaction during the first lithiation process.<sup>39</sup> The peak at around 2.0 V during the following charge step is attributed to the delithiation process of Li<sub>2</sub>FeS<sub>2</sub> to form Li<sub>2-x</sub>FeS<sub>2</sub>. Worthy of noting, the electrochemical behaviour of the FeS microsHEET networks electrode is largely sustained in the following cycles, with gradual changes in intensity of the peaks. Chen *et al.*<sup>14</sup> indicated that the conversion between Li<sub>2</sub>FeS<sub>2</sub> and Li<sub>2-x</sub>FeS<sub>2</sub> is reversible, which enables the application of iron sulfides in rechargeable LIBs.

Charge/discharge voltage profiles of FeS microsHEET networks electrode at 0.1 A g<sup>-1</sup> are shown in Fig. 5b and are in agreement with the CV curves. There are two plateaus during the first discharge, which are similar to those reported previously in the literature.<sup>14</sup> The electrode delivers a high initial discharge capacity of 772 mAh g<sup>-1</sup> and a charge capacity of 679 mAh g<sup>-1</sup>, leading to a first-cycle Columbic efficiency of 87.9%. It is well-known that the irreversible capacity loss during the first cycle arises due to inevitable formation of SEI film and electrolyte decomposition. During the second cycle, the FeS microsHEET networks electrode delivers a discharge capacity of 697 mA g<sup>-1</sup> and a charge capacity of 674 mAh g<sup>-1</sup> with a much higher Columbic efficiency of 96.7%. What is more, FeS microsHEET networks exhibits a narrow voltage hysteresis as confirmed by the

50 closer discharge/charge voltage profiles.

The discharge/charge cycling stability of FeS microsHEET networks and microspheres electrodes were examined at a current density of 0.1 A g<sup>-1</sup> between 0.01 and 3.0 V (Fig. 5c). The discharge capacity of the FeS microsHEET networks electrode is 772 mAh g<sup>-1</sup> at the 1<sup>st</sup> cycle and remains at 677 mAh g<sup>-1</sup> at the 20<sup>th</sup> cycle, indicating a stable cycling characteristic. As comparison, FeS microspheres anode delivers a discharge capacity of 743 mAh g<sup>-1</sup> at the 1<sup>st</sup> cycle and a lower capacity of 233 mAh g<sup>-1</sup> at the 20<sup>th</sup> cycle. These results reveal that FeS microsHEET networks exhibited much higher lithium-ion storage capacity and much better cyclic performance than FeS microsphere films. FeS microspheres exhibit the poor electrochemical performance, a possible reason is that the poor electric contact between the microspheres and current collector (Fig. 3a), decreasing the amount of effective substance during cycles. The high capacity performance of FeS microsHEET is superior to that of most FeS electrodes previously reported, including pristine FeS-embedded carbon microspheres and bare FeS nanocrystals.<sup>14, 21</sup>

To better understand the advantage of the FeS microsHEET arrays in lithium storage, the rate performance of the FeS microsHEET arrays electrode is also investigated (Fig. 5d). It depicts tenth-cycle discharge capacities of around 797, 770, 505 and 357 mAh g<sup>-1</sup> at current densities of 0.1, 0.2, 0.5 and 1 A g<sup>-1</sup>, respectively. Even at the current density of 2 A g<sup>-1</sup>, the FeS microsHEET arrays still delivered a tenth-cycle discharge capacity of 150 mAh g<sup>-1</sup>, which are about two times larger than those reported of the powder FeS electrode at 2 A g<sup>-1</sup>.<sup>19</sup> As the current density returns to the initial value of 0.1 A g<sup>-1</sup>, the electrode resume a capacity of 593 mAh g<sup>-1</sup>, indicating that the electrode has lost some capability and shows a certain decline of performance during high rate discharges.

As shown in Fig. 5e, after 20 cycles, the microsheets are thickened to some degree resulting from the repeating lithiation and delithiation reactions. Part space between the original open-structures between the FeS microsheets is filled with a little reaction products remaining from the lithiation and delithiation process, which may lead to a slight irreversible capacity loss.<sup>40, 41</sup> However, the structural integrity of the FeS microsHEET array is well preserved. The enhanced structure stability should be attributed to the unique architecture of net-structured microsHEET array.

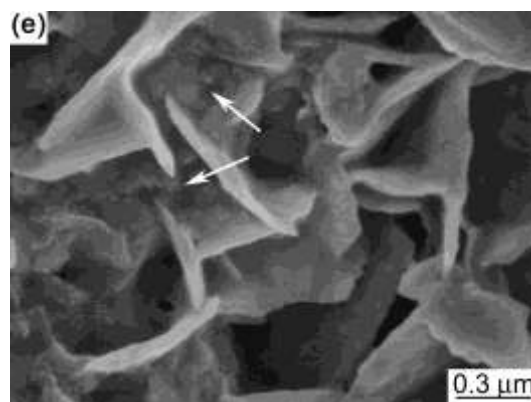
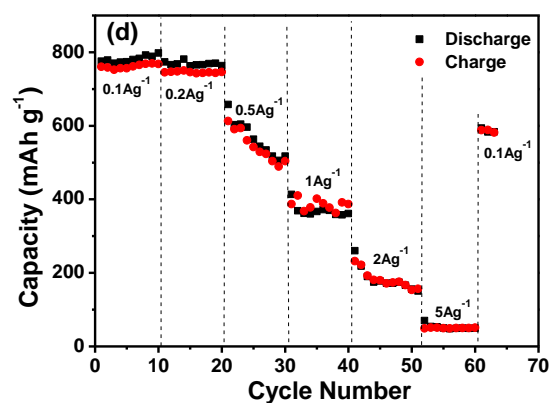
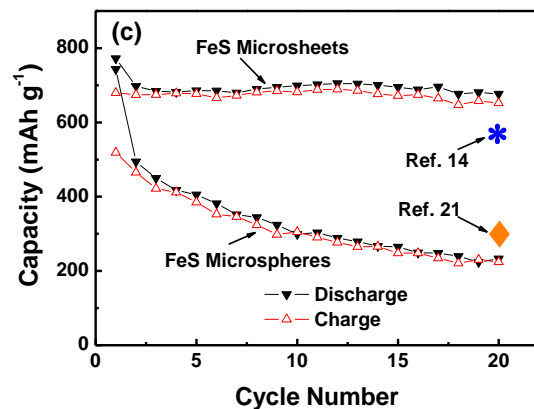
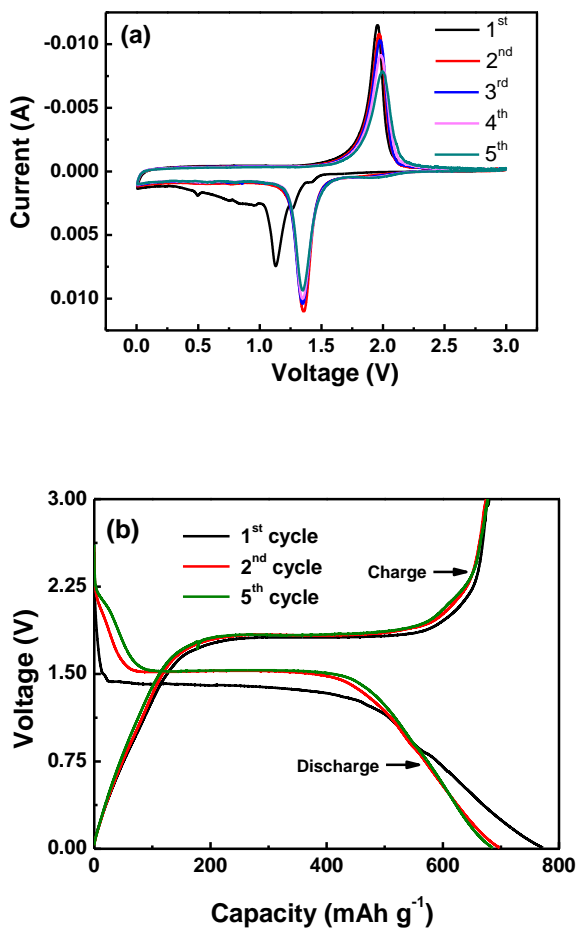
Compared with FeS microsphere or nanoparticle films, FeS microsHEET networks possess a much better electrochemical performance for lithium-ion batteries, which could be deduced from their morphologies and structures due to following advantages:

(1) The microsHEET structure greatly shortens the ionic diffusion length and provides sufficient electrode-electrolyte contact area for lithium-storage reactions (Fig. 5f).<sup>39, 42, 43</sup> Furthermore, the CV peak shape of FeS microsHEET networks was sharp and intense (Fig. 5a), demonstrating that the products have low overall resistance and great efficiency of the redox reaction. The low voltage hysteresis (Fig. 5b) should result in faster kinetics and improved energy efficiency.

(2) The FeS microsheets are interconnected with each other to form macropores, which can effectively accommodate large

volume change induced by the  $\text{Li}^+$  intercalation/excalation (Fig. 5f). Therefore, the structural integrity could be well remained during the discharge/charge processes (Fig. 5e).<sup>44,45</sup>

(3) Compared with the fabrication of the traditional battery electrode, *in-situ* growth of microsheet networks onto the metal current collector results in good electrical contact of every microsheet with the metal current collector. That should be beneficial for easier transportation for electrons and lithium ions, and good strain accommodation.<sup>46,47</sup> What's more, no additive is needed for the preparation of electrode.



15

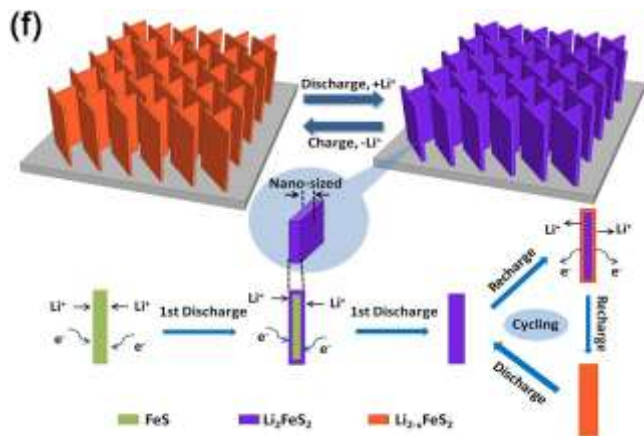


**Fig.5** (a) CV results of the FeS microsheet networks electrode at a scan rate of 0.1 mV s<sup>-1</sup>; (b) charge-discharge voltage profiles of the FeS microsheet networks with a current density of 0.1 A g<sup>-1</sup>; (c) comparison of the cycling performance of FeS microsheet networks electrode and FeS microspheres electrode at 0.1 A g<sup>-1</sup>; (d) cycling performance of the FeS microsheet networks electrode at various current densities; (e) FESEM images of the FeS microsheet networks after the discharge-charge of 20 cycles, white arrows point out that some open-structure is filled with reaction product; (f) schematic transformation of the FeS microsheet networks cathode during electrochemical cycling.

### 3 Conclusions

In summary, FeS microsheet networks on flexible iron foil were prepared in the presence of EDA via a solution-based synthesis technique. As a donor ligand, EDA has a significant effect on the controlling of the crystal growth, leading to the formation of uniform FeS microsheet networks. With adjustable synthesis conditions, FeS microspheres can also be obtained. The mackinawite FeS microsheet networks are the first time used as electrode in LIB and deliver promising Li capacity (772 mAh g<sup>-1</sup> at the 1<sup>st</sup> cycle and 677 mAh g<sup>-1</sup> at the 20<sup>th</sup> cycle), exhibiting much higher capacity properties and better cyclic performance than FeS microspheres. The excellent performance of the FeS microsheet networks can be attributed to the layered structure of the FeS microsheet networks having larger electrode-electrolyte contact area, shorter ionic diffusion length and easier transportation of lithium ions. Thus, compared to traditional electrodes, this nanostructured films on metal foils could be a promising electrode materials for the practical use in the next generation lithium-ion batteries.

### 4 Experimental Section

**Fabrication of FeS microsheet networks:** The growth of FeS on the Fe substrate was carried out via the general solution route. The FeCl<sub>3</sub>·6H<sub>2</sub>O (0.5 mmol), Na<sub>2</sub>S·9H<sub>2</sub>O (2 mmol) and S (2 mmol) were dissolved in 30 mL DI water to form a homogenous solution. Then, 10 mL of EDA was added while stirring continued. Afterwards, the mixture was transferred into a 50 mL Teflon-lined autoclave (filled up to 80% of its total volume) and then the Fe foil was placed standing against the wall. The autoclave was sealed, heated to 160 °C for 12 h, and then cooled

to room temperature. The foil covered with reaction products was collected from the solution, rinsed with distilled water and absolute ethanol by ultrasonication, and dried in an oven at 60 °C for 5 h. Finally, the products were heated at 250 °C for 2 h in vacuum (~10<sup>-3</sup> Torr) furnace to form FeS. The amounts of the FeS on the metal collector substrate were accurately examined using a microbalance. The resolution of the weight is 0.1 mg.

**Fabrication of FeS microspheres:** FeCl<sub>3</sub>·6H<sub>2</sub>O (0.5 mmol) and Tu (2 mmol) were added in 30 mL DI water to form a homogenous solution. Then the solution was added into a 30 mL Teflon-lined autoclave with a piece of clean iron foil-placed standing against the wall. The autoclave was heated at 160 °C for 12 h and cooled down to room temperature. The iron foil was taken out and thoroughly rinsed with distilled water and absolute ethanol, and finally dried for characterization.

**Characterization:** All observation and characterization were performed and analyzed on the face side. The structural characteristic of the samples was tested by X-ray diffraction diffractometer (XRD, X'Pert PRO) using Cu K $\alpha$  radiation. The data were collected from 2 $\theta$  = 10-90° in a step-scan mode. The morphologies of the samples were investigated by a field-emission scanning electron microscopy (FESEM, Hitachi SU-70). The substrate-bound iron sulfide were scraped from the Fe foil mechanically, dispersed in an alcohol solution ultrasonically and then deposited on carbon-coated copper grids for high resolution transmission electron microscope (HRTEM, JEM-2100) characterization.

**Electrochemical properties:** The coin-type cells were assembled in a glove box filled with pure argon gas directly using the FeS grown on iron substrate as the cathode without any ancillary materials and lithium metal as the anode. Both the cathode and anode were electronically separated by a polypropylene film saturated with 1 M LiPF<sub>6</sub> electrolyte solution made up of 1: 1 w/w diethyl carbonate and ethylene carbonate. Charge-discharge cycles were performed in the potential range of 0.01 and 3.0 V at room temperature using a multichannel battery test system (Newware, BST-610). Cyclic voltammetry (0-3 V, scan rate of 1 mV s<sup>-1</sup>) was carried out with an electrochemical workstation (Solartron).

### Acknowledgements

The project is supported by the National Natural Science Foundation of China (Grant No. 21373184), Zhejiang Provincial Natural Science Foundation of China under Grant No. LR14B060002 and LQ12B01001, Public Projects of Zhejiang Province (Grant No. 2012C31023).

### Notes and references

- <sup>1</sup> Chengcheng Xing and Dan Zhang contributed equally  
<sup>a</sup> College of Materials Science and Engineering, Zhejiang University, Hangzhou 310027, China. Fax: +86 57187953134; Tel: +86 57187953134; E-mail: liujiabin@zju.edu.cn; yzjiang@zju.edu.cn.  
<sup>b</sup> College of Materials and Environmental Engineering, Hangzhou Dianzi University, Hangzhou 310018, China

†Electronic Supplementary Information (ESI) available: [details of any supplementary information available should be included here]. See DOI: 10.1039/b000000x/

## References

- 1 S. G. Sorensen, H. G. Fuchtbauer, A. K. Tuxen, A. S. Walton and J. V. Lauritsen, *ACS Nano*, 2014, **8**, 6788-96.
- 2 G. D. Park, S. H. Choi, J. K. Lee and Y. C. Kang, *Chem.-Eur. J.*, 2014, **20**, 12183-9.
- 3 J. Wang, D. L. Chao, J. L. Liu, L. L. Li, L. F. Lai, J. Y. Lin and Z. X. Shen, *Nano Energy*, 2014, **7**, 151-60.
- 4 X. M. Wu, S. C. Zhang, H. Fang, Z. J. Du and R. X. Lin, *J. Power Sources*, 2014, **264**, 311-9.
- 5 B. T. Yonemoto, G. S. Hutchings and F. Jiao, *J. Am. Chem. Soc.*, 2014, **136**, 8895-8.
- 6 N. Li, X. L. Zhang, S. T. Chen, W. Yang, H. Z. Kang and W. H. Tan, *CrystEngComm*, 2011, **13**, 6549-54.
- 7 W. K. Koh, C. B. Murray, A. C. Bartnik and F. W. Wise, *J. Am. Chem. Soc.*, 2010, **130**, 3909-13.
- 8 I. T. Sines, D. D. Vaughn, R. Misra, E. J. Popczun and R. E. Schaak, *J. Solid State Chem.*, 2012, **196**, 17-20.
- 9 A. Paoletta, C. George, M. Povia, Y. Zhang, R. Krahne, M. Gich, A. Genovese, A. Falqui, M. Longobardi, P. Guardia, T. Pellegrino and L. Manna, *Chem. Mater.*, 2011, **23**, 3762-8.
- 10 X. Yang, W. Q. Liu, M. Xiong, Y. Y. Zhang, T. Liang, J. T. Yang, M. S. Xu, J. Ye and H. Z. Chen, *J. Mater. Chem. A*, 2014, **2**, 14798-806.
- 11 N. Liu, P. Kim, J. H. Kim, J. H. Ye, S. Kim and C. J. Lee, *ACS Nano*, 2014, **8**, 6902-10.
- 12 X. Xu, Z. Y. Fan, S. J. Ding, D. M. Yu and Y. P. Du, *Nanoscale*, 2014, **6**, 5245-50.
- 13 Y. Liu, W. Wang, H. B. Huang, L. Gu, Y. W. Wang and X. S. Peng, *Chem. Commun.*, 2014, **50**, 4485-8.
- 14 C. Xu, Y. Zeng, X. H. Rui, N. Xiao, J. X. Zhu, W. Y. Zhang, J. Chen, W. L. Liu, H. T. Tan, H. H. Hng and Q. Y. Yan, *ACS Nano*, 2012, **6**, 4713-21.
- 15 R. Nakamura, A. Okamoto, N. Tajima, G. J. Newton, F. Kai, T. Takashima and K. Hashimoto, *ChemBioChem*, 2010, **11**, 643-5.
- 16 H. Y. Jeong, B. Klaue, J. D. Blum and K. F. Hayes, *Environ. Sci. Technol.*, 2007, **41**, 7699-705.
- 17 G. L. Henriksen and D. R. Vissers, *J. Power Sources*, 1994, **51**, 115-28.
- 18 L. Fei, Y. F. Jiang, Y. Xu, G. Chen, Y. L. Li, X. Xu, S. G. Deng and H. M. Luo, *J. Power Sources*, 2014, **265**, 1-5.
- 19 Y. R. Wang, H. T. Liao, J. Wang, X. F. Qian, Y. C. Zhu and S. Q. Cheng, *Int. J. Electrochem. Sci.*, 2013, **8**, 4002-9.
- 20 T. A. Yersak, T. Evans, J. M. Whiteley, S. B. Son, B. Francisco, K. H. Oh and S. H. Lee, *J. Electrochem. Soc.*, 2014, **161**, A663-A7.
- 21 B. Wu, H. H. Song, J. S. Zhou and X. H. Chen, *Chem. Commun.*, 2011, **47**, 8653-5.
- 22 D. Bernardi and J. Newman, *J. Electrochem. Soc.*, 1987, **134**, 1309-18.
- 23 A. Netz, R. A. Huggins and W. Weppner, *J. Power Sources*, 2003, **119**, 95-100.
- 24 F. C. Zheng, D. Q. Zhu and Q. W. Chen, *ACS Appl. Mater. Interfaces*, 2014, **6**, 9256-64.
- 25 Y. X. Yu, X. Y. Liu, X. H. Xia, Q. Q. Xiong, X. L. Wang, C. D. Gu and J. P. Tu, *Mater. Res. Bull.*, 2014, **51**, 112-8.
- 26 X. Q. Qiu, M. Liu, T. Hayashi, M. Miyauchi and K. Hashimoto, *Chem. Commun.*, 2013, **49**, 1232-4.
- 27 D. Rickard and G. W. Luther, *Chem. Rev.*, 2007, **107**, 514-62.
- 28 D. W. Wang, Q. H. Wang and T. M. Wang, *CrystEngComm*, 2010, **12**, 755-61.
- 29 R. Romano-Trujillo, E. Rosendo, M. Ortega, A. Morales-Sanchez, J. M. Gracia, T. Diaz, G. Nieto, G. Garcia, J. A. Luna-Lopez and M. Pacio, *Nano Technol.*, 2012, **23**, 185602-7.
- 30 S. H. Yu and M. Yoshimura, *Adv. Funct. Mater.*, 2002, **12**, 277-85.
- 31 R. J. Davey, S. N. Black, L. A. Bromley, D. Cottier, B. Dobbs and J. E. Rout, *Nature*, 1991, **353**, 549-50.
- 32 C. H. Lai, K. W. Huang, J. H. Cheng, C. Y. Lee, B. J. Hwang and L. J. Chen, *J. Mater. Chem.*, 2010, **20**, 6638-45.
- 33 F. Lu, W. P. Cai, Y. G. Zhang, Y. Li, F. Q. Sun, S. H. Heo and S. O. Cho, *J. Phys. Chem. C*, 2007, **111**, 13385-92.
- 34 C. H. Lai, K. W. Huang, J. H. Cheng, C. Y. Lee, W. F. Lee, C. T. Huang, B. J. Hwang and L. J. Chen, *J. Mater. Chem.*, 2009, **19**, 7277-83.
- 35 H. Grijalva, M. Inoue, S. Boggavarapu and P. Calvert, *J. Mater. Chem.*, 1996, **6**, 1157-60.
- 36 B. C. Kim, K. Takada, N. Ohta, Y. Seino, L. Q. Zhang, H. Wada and T. Sasaki, *Solid State Ionics*, 2005, **176**, 2383-7.
- 37 Y. Kim and J. B. Goodenough, *J. Phys. Chem. C*, 2008, **112**, 15060-4.
- 38 E. Strauss, D. Golodnitsky and E. Peled, *Electrochim. Acta*, 2000, **45**, 1519-25.
- 39 X. H. Wang, Y. Fan, R. A. Susantyoko, Q. Z. Xiao, L. M. Sun, D. Y. He and Q. Zhang, *Nano Energy*, 2014, **5**, 91-6.
- 40 T. Okumura, M. Shikano and H. Kobayashi, *J. Mater. Chem. A*, 2014, **2**, 11847-56.
- 41 Y. Kim, J. H. Lee, S. Cho, Y. Kwon, I. In, J. Lee, N. H. You, E. Reichmanis, H. Ko, K. T. Lee, H. K. Kwon, D. H. Ko, H. Yang and B. Park, *ACS Nano*, 2014, **8**, 6701-12.
- 42 R. Thomas, K. Y. Rao and G. M. Rao, *Electrochim. Acta*, 2013, **108**, 458-64.
- 43 S. Huang, Y. Lu, T. Q. Wang, C. D. Gu, X. L. Wang and J. P. Tu, *J. Power Sources*, 2013, **235**, 256-64.
- 44 J. P. Liu, Y. Y. Li, X. T. Huang, R. M. Ding, Y. Y. Hu, J. Jiang and L. Liao, *J. Mater. Chem.*, 2009, **19**, 1859-64.
- 45 B. L. Cao, Y. Jiang, C. Wang, W. H. Wang, L. Z. Wang, M. Niu, W. J. Zhang, Y. Q. Li and S. T. Lee, *Adv. Funct. Mater.*, 2007, **17**, 1501-6.
- 46 H. K. Song, K. T. Lee, M. G. Kim, L. F. Nazar and J. Cho, *Adv. Funct. Mater.*, 2010, **20**, 3818-34.
- 47 J. Liu, G. Z. Cao, Z. G. Yang, D. H. Wang, D. Dubois, X. D. Zhou, G. L. Graff, L. R. Pederson and J. G. Zhang, *ChemSusChem*, 2008, **1**, 676-97.
- 48 X. Y. Zhao, B. Liu, C. W. Hu and M. H. Cao, *Chem.-Eur. J.*, 2014, **20**, 467-73.